Electronic Supplementary Information

Microfibrous Entrapment of Ni/Al$_2$O$_3$ For Dry Reforming of Methane: A Demonstration on Enhancement of Carbon Resistance and Conversion

Wei Chen,[a] Wenqian Sheng,[a] Guofeng Zhao,[a] Fahai Cao,[b] Qingsong Xue,[a] Li Chen[a] and Yong Lu*[a]

[a] Shanghai Key Laboratory of Green Chemistry and Chemical Processes, Department of Chemistry, East China Normal University, Shanghai 200062, China

[b] College of Chemical Engineering, East China University of Science and Technology, Shanghai 200237, China

Fax: (+86)21-62233424, **E-mail:** ylu@chem.ecnu.edu.cn (Y. Lu.)

S1. Materials and Methods

S1.1. Preparation

Sintered microfibrous entrapped 0.15-0.18 mm dia. γ-Al_2O_3 support particles (Alfa Aesar,USA) using copper fibers (8 μm in dia. by 2-3 mm length) were prepared through wet-lay paper making method, followed by sintering in a H_2 atmosphere.[S1,S2] In this process, 1.7 g of cellulose (20–40 mm dia. by 2-3 mm length) and 5.0 g of copper fibers were added into a commercial blender which was filled with 1.5 L water, and blended vigorously to produce a uniform suspension. The suspension as well as 7.5 g of Al_2O_3 support particulates were transferred into the headbox of a 159 mm dia. circular sheet former (ZCX-159A, made in China) filled with 8.5 L water under manual mixing. The 159 mm circular preform was then formed by draining, pressing at ~400 kN m^{-1}, and drying at 373 K overnight. As-made paper with entrapped the Al_2O_3 support particulates was, then, pre-oxidized in air at 573 K to remove the cellulosic binders, followed by sintering in H_2 at 1173 K for 1 h

Active Ni was highly dispersed onto the pore surface of γ-Al_3O_3 by incipient wetness impregnation method, using its nitrate salts as precursors. The impregnated samples (Cu-microfibrous entrapped Ni/Al_2O_3 (Cu-MFE-Ni/AlO) composite) were dried at 383 K overnight and followed by calcination at 523 K for 1 h prior to packing into the reactor. A piece of 11.50 g as-made Cu-MFE-Ni/AlO consists of 4.78 g of copper fibers and 6.72 g of Ni/Al_2O_3 particles. By the means of ICP-AES (Thermo Scientific iCAP 6300 ICP-AES), the Ni content is determined to be 10.9 wt% for the Ni/Al_2O_3 catalyst entrapped in the Cu-microfibrous structure. Note that the Ni/AlO particles packed in the packed bed (PB) were taken from Cu-MFE-Ni/AlO composite by unlocking the network, making sure that the catalyst particles were same in both the microfibrous composite bed and the PB.

S1.2. Characterization

The images of MFEC were taken by an Olympus zoom stereomicroscope (SZ61) and by a FE-SEM instrument (Hitachi S-4800). The surface area was determined on a Quantromn Autosorb 3B gas adsorption analyzer, using N_2 physisorption at its boiling temperature. The exact composition of the samples was determined by using a Thermo Scientific iCAP 6300 ICP-AES.

S1.3. Reaction evaluation

Testing experiments on DRM using the MFEC with entrapping Ni/Al_2O_3 particles and individual Ni/Al_2O_3 catalyst particles were carried out in a quartz tubular reactor (having an inner diameter of 16 mm) heated by a temperature-controlled tube furnace at atmospheric pressure. In the case of MFEC testing, 5 pieces of Cu-MFE-Ni/AlO circular disks (containing ~0.3 g of Ni/Al_2O_3 particles) were punched out from their large sheet to fit the i.d. (16 mm) of the reactor tube and layer-by-layer packed into the reactor tube to 5 mm of thickness. The disks were 1 mm bigger in dia. (17 mm) than the reactor tube, which can offer a good seal at the reactor wall as well as a good contact for a high inside wall heat transfer coefficient. In the case of PB, 0.3 g of Ni/AlO particles was charged for testing. The catalysts were reduced in a flow of H_2 (99.999 purity) at 1173 K for 2 h before an equimolar feed gas of CH_4 (99.99% purity) and CO_2 (99.995% purity) was introduced into the catalyst bed. The total GHSV (based on the weight of Ni/Al_2O_3 particles) was 20,000 mL $h^{-1}g_{cat}^{-1}$, and the temperature were in range of 873-1173 K, respectively. The reactant and product gas was analyzed by using an HP 6850 GC equipped with TCD connected to Plot Q and MS 5A parallel capillary column combo (DIKMA). Each condition had been run for 1 h before the data were collected.

To elucidate the effectiveness of heat transfer intensification of Cu-fiber, a set of beds were elaborately prepared for catalytic tests. And the characteristics of each beds are summarized in Table 1S. Bed A was packed with ~0.3 (equal to the amount of that in Cu-MFE-Ni/AlO bed) g of Ni/AlO particles. Bed B was packed with equivalent amount (~0.3 g) of catalyst particles as those packed in A, and diluted with 0.15~0.18 mm alumina to the equivalent volume as that of bed C. Bed C was Cu-MFE-Ni/AlO as described in **S1.1**, and was represented the base case. Bed D was sandwiched equivalent amount of catalysts as those entrapped into bed D with bottom and top pieces of microfibrous mesh. Bed E was packed with equivalent amount of Cu-microfibrous mesh as those used in bed C without any further treatment to verify the catalytic activity of copper-fibers.

Table 1 Characteristics of various reaction beds[a]

Bed ID	A	B	C	D	E
Bed type	Packed	Diluted	Cu-MFE-Ni/AlO	Sandwiched	Cu-fiber
Cu-fiber (vol%/wt%)	0.0/0.0	0/0	2.0/41.1	2.1/42.3	3.9/100
Ni/Al_2O_3 (vol%/wt%)	61.8/0.3	64.4/0.3	26.7/58.9	27.2/57.7	0/0
Voidage (vol%)	33.2	35.6	71.3	70.7	96.1
Ni/Al_2O_3 size (mm)	0.15~0.18	0.15~0.18	0.15~0.18	0.15~0.18	-
Bed density (g cm^{-3})	0.58	0.52	0.43	0.42	0.35

[a] Each reaction condition was run for 2 h, during which the experimental data were collected.

S1.4. Results
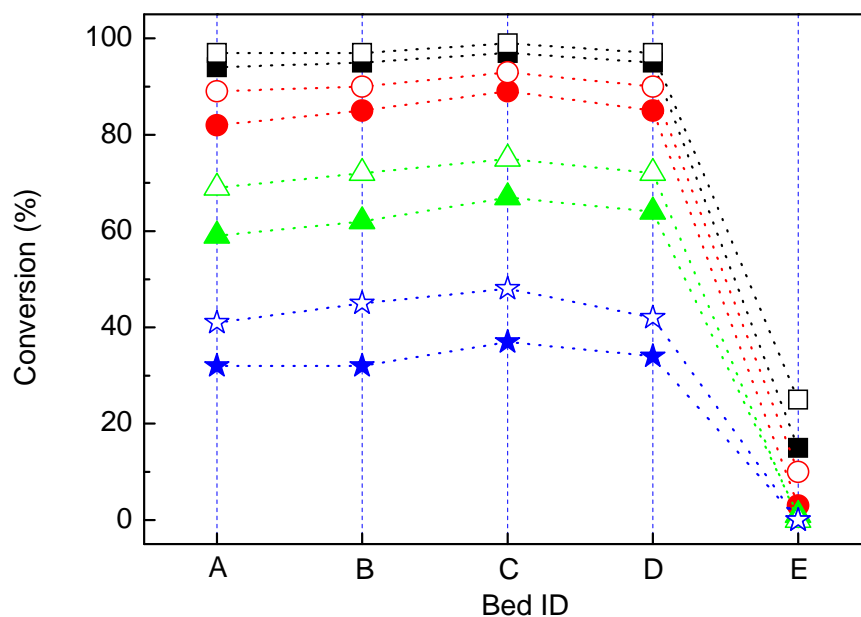
Fig. S1 CH_4 (solid) and CO_2 (hollow) conversions for DRM reaction over various beds at 1173 K (square), 1073 K (circle), 973 K (triangle), and 873 K (star).

Bed B and D were designed to distinguish the benefit from the enhanced thermal conductivity of bed C in equivalent bed volume. Catalyst particles loaded were separated by γ-Al_2O_3 particles and copper-fibers in bed B and bed C, respectively. The particles packed in bed D were not connected by copper microfibrous structure, though the copper meshes were placed at both top and bottom of catalyst particles bed. Undoubtedly, the 3D copper-fiber network with high thermal conductivity can conduct heat flow more easily and rapidly than the porous Al_2O_3 particles do. This is essentially desirable for the highly endothermic DRM that required a lot of heat on the catalyst surface. As a result, an increase in the steady-state reactor conversion was obtained by using the 3D copper-fiber network entrapment technology. For example, at 1073 K the reactor conversions were: 93% CO_2 and 89% CH_4 for Cu-MFE-Ni/AlO vs. 89% CO_2 and 82% CH_4 for the PB (Fig. 1S). While, the results of bed F indicated that the neat Cu-fiber exhibited rather low activity. So, the Cu-fiber can definitely be considered as intensifier in the catalytic bed rather than the co-catalyst.

S2. Tests

S2.1. Pressure drop determination

Pressure drop through the MFEC bed was measured using a sample cell consisting of a 19 mm (i.d.) tube fitting with 14 mm (i.d.) transparent plastic tubing inserted into the ends of the fitting. The detailed process was described in detail elsewhere[S1] by using a Magnehelica 20000-250 PA differential pressure gauge (Dwyer, USA).

According to Darcy's law (Eq. S1), which is a simple proportional relationship between the instantaneous discharge rate through a porous medium, the viscosity of the fluid and the pressure drop over a given distance[S3], the pressure drop should be a linear function of the flow rate through the porous media when the Re_p was smaller than 10. So the second term in Ergun's equation (Eq. S2)[S4], which was suitable for predicting the pressure drop in PB with the medium of 50% or less porosity when the Reynolds number was in the range of 0.4-1000, could be neglected accordingly for the reason that the Re_p was quite small in the present case.

$$\frac{\Delta P}{L} = \frac{\mu_f}{K} u_f \tag{S1}$$

$$\frac{\Delta P}{L} = C_1 \frac{(1-\varepsilon_b)^2}{\varepsilon_b^{\ 3} d_p^{\ 2}} \mu_f u_f + C_2 \frac{(1-\varepsilon_b)}{\varepsilon_b^{\ 3} d_p} \rho_f u_f^{\ 2} \tag{S2}$$

The pressure drop in MFEC was fitted by M-PMP equation (Eq. S3),[S5] which was obtained by modifying the PMP equation[S6] developed for predicting the pressure drop through the microfibrous materials:

$$\frac{\Delta P}{L} = C_1 \frac{\tau^2}{\gamma^2} \frac{\mu(1-\varepsilon)^2}{\varepsilon^3} \left[\left(\sum \frac{X_i}{\phi_i D_i} \right)^2 + X_{FD} \sum \frac{X_i}{(\phi_i D_i)^2} \right] u_f \tag{S3}$$

S2.2. Results of pressure drop determination
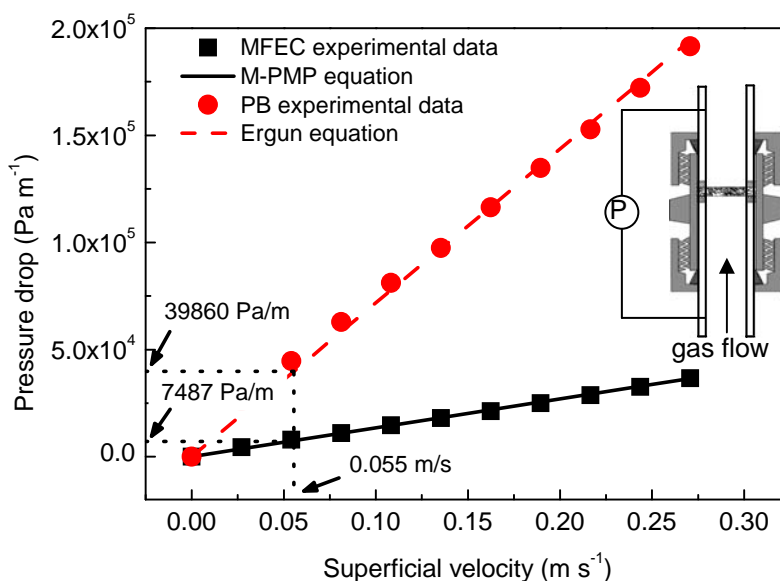
Fig. S2   Profiles of pressure drop per meter as a function of superficial velocity in PB and Cu-MFE-Ni/AlO.

   The Cu-MFE- Ni/AlO bed with high voidage (70 vol%) exhibited much higher permeability than PB did. As the gas flow rate increased within the range we tested, the pressure drops in both Cu-MFE-Ni/AlO and PB were increased linearly, which was well consistent with Darcy's law (Eq. S1).[S3] Clearly, in both Cu-MFE-Ni/AlO and PB there has a simple proportional relationship between the instantaneous discharge rate through a porous medium, the viscosity of the fluid and the pressure drop over a given distance. The pressure drop in PB and Cu-MFE-Ni/AlO were fitted by Ergun's equation (Eq. S2)[S4] and M-PMP equation (Eq. S3),[S5] respectively. In the case of DRM at temperature of 1073 K, feedstock of 100 mL min^{-1}, and conversion of ~89%, the superficial velocity was about 0.055 m s^{-1} in this hot bed region. At this axial velocity, as indicated in Fig. S1, the pressure drop of the Cu-MFE-Ni/AlO composite bed was 7487 P am^{-1}, only about a fifth that (39860 Pa m^{-1}) of the PB.

S3. CFD calculation

S3.1. Modeling
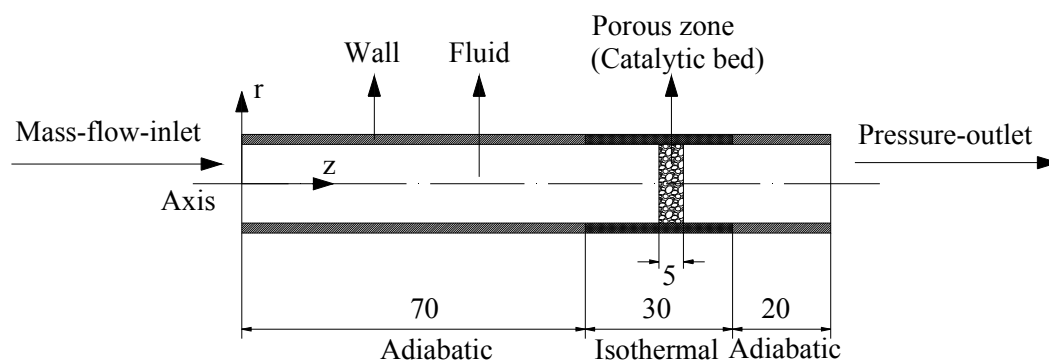
Fig. S3 Schematic diagram of the system modeled by 'FLUENT'

The commercial CFD code 'FLUENT' was employed to obtain the temperature distribution at steady state inside the catalytic bed. The schematic diagram of the system modeled was shown in Fig. S2. A premixed (equimolar) and preheated (500 K) feed gas of CH_4 and CO_2 was introduced into the tube by using the mass-inlet condition of 2.05×10^{-6} kg s^{-1}. The catalytic bed contacting to the isothermal wall was initially at a uniform temperature of 1073 K. The reactant was reheated by the reactor wall when it traveled in the tube before it diffused into the bed. All the thermophysical properties of the materials (solids and gases) are functions of the local temperature and composition.

8

S3.2. Conservation equations

Two modes of heat transfer (conduction and convection, while the radiation was omitted) were controlled by the governing conservation equation of energy (Eq. S4).

$$\frac{\partial}{\partial t}(\varepsilon_b \rho_f E_f + (1-\varepsilon_b)\rho_s E_s) + \nabla \cdot (\vec{u}(\rho_f E_f + p)) = \nabla \cdot \left[k_e \nabla T - \left(\sum_i h_j J_j \right) + (\overline{\overline{\tau}}_f \cdot \vec{u}_f) \right] + S_f \qquad \text{(S4)}$$

Boundary condition:

At $z = 0$, $T_f(r, z) = T_{inlet}$;

From $z = 70$ to $z = 100$: T_{wall} = reaction temperature (1073 K);

$$\frac{\partial T_f(r,z)}{\partial r}\bigg|_{r=0} = \frac{\partial T_b(r,z)}{\partial r}\bigg|_{r=0} = 0 \, ;$$

$$k_{e,r} \frac{\partial T(r,z)}{\partial r}\bigg|_{r=R} = h_w (T_w - T_f(R,z)) \, ;$$

Where k_e is the effective thermal conductivity in the porous medium, and is calculated by 'FLUENT' as the volume average of the fluid conductivity and the solid conductivity (Eq. S5):

$$k_e = \varepsilon_b k_f + (1-\varepsilon_b)k_s \qquad \text{(S5)}$$

According to Tatarchuk's work,[S7] the effective thermal conductivity of MFEC is anisotropic. The k_r is approximately 5 times of the value of k_z, because most of the metallic fibers preferentially lie in *x-y* plane, such that few metal fibers are along the axial direction in MFEC. In addition, the catalytic bed was stacked by separate disks with 0.15 mm of thickness.

The two terms on the left side of the Eq. S4 represent the energy accumulating rate and energy flux into; and the first three terms on the right side of Eq. S4 represent the energy transfer due to conduction, species diffusion, and viscous dissipation, respectively. However, viscous dissipation can be neglected because of the low viscosity of gas flow. S_f , given by Eq. S6, stands for the energy source due to volumetric reaction R_j, which will be discussed later.

$$S_f = \sum_{j'} \left[\frac{h_j^0}{M_j} + \int_{T_{ref,j}}^{T_j} c_p dT \right] R_j \qquad \text{(S6)}$$

The species transport could be controlled by the species conservation equation:

$$\frac{\partial}{\partial t}(\rho_f Y_j) + \nabla \cdot (\rho_f u_f Y_j) = -\nabla \cdot \overline{J}_j + R_j \qquad \text{(S7)}$$

Boundary condition

From $z = 0$ to $z = 85$: $Y_{CH4} = Y_{CH4,inlet}$; $Y_{CO2} = Y_{CO2,inlet}$

From $z = 90$ to $z = 120$: $Y_{CH4} = Y_{CH4,outlet}$; $Y_{CO2} = Y_{CO2,outlet}$; $Y_{CO} = Y_{CO,outlet}$; $Y_{H2} = Y_{H2,outlet}$

Here J_i is the diffusion flux of species i, which arises due to concentration gradients. The diffusion coefficient D was calculated by Edward's method.[S8] Density ρ_i was determined by ideal gas law. Mass fraction of the species Yj at outlet was determined experimentally (see Fig. S3).

The gas flow in the tube was treated as laminar flow considering the Reynolds number in this case was smaller than 5. So, in the description of pressure drop in the porous zone (Eq. S8), the second term arising from inertial was negligible. And the viscous loss term $1/\alpha$ can be derived from Ergun's equation (Eq. S2) or M-PMP equation (Eq. S3)).

$$\frac{\Delta P}{L} = \frac{\mu_f}{\alpha} u_f + C_2 \frac{1}{2} \rho_f \left| u_f \right| u_f \qquad (S8)$$

S3.3. Reaction

The heat obtained from catalytic reaction was so complex that the following simplified model was employed to complete the energy equation. The finite-rate volumetric reaction model was used to determine the reaction heat, and the reaction rate was approximately calculated as (Eq. S9):

$$R_j = \nu_j A \exp(\frac{-Ea}{RT})[C_{CH_4}]^{n_{CH4}}[C_{CO_2}]^{n_{CO_2}} \qquad (S9)$$

Here, the apparent activation energy *Ea* (61.95 kJ/mol) was determined experimentally as shown in Fig. S3, and values were consistent with the Bradford's summary.[S9]
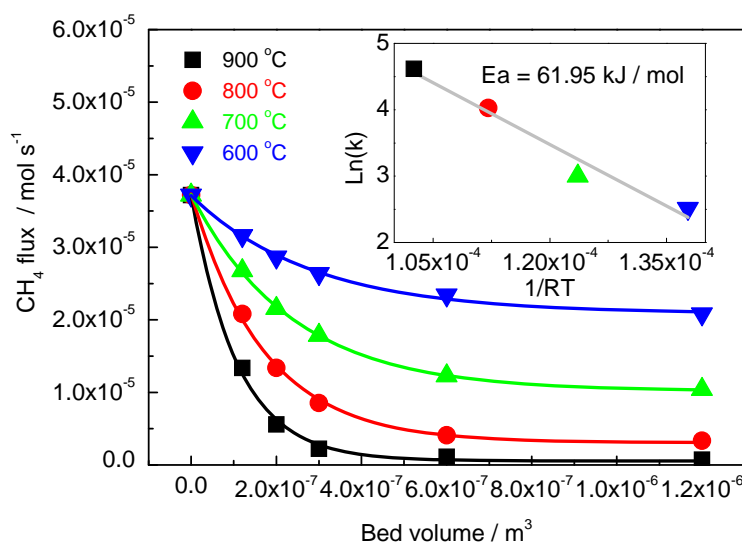
Fig. S4 CH$_4$ flux along the axial direction of catalytic bed at 1173 K (square), 1073 K (circle), 973 K (up-triangle), and 873 K (down-triangle). Inset: apparent activation energy.

S3.4. Parameters of materials employed in calculation

	Voidage (%)	k_{er} / W m^{-1} K^{-1}	k_{ez} / W m^{-1} K^{-1}
MFEC	0.713	24.9	5.11
PB	0.332	1.15	1.15

S3.5. Result

The temperature difference from reactor wall to central line was about 50 K for MFEC, compared to ~170 K for PB.
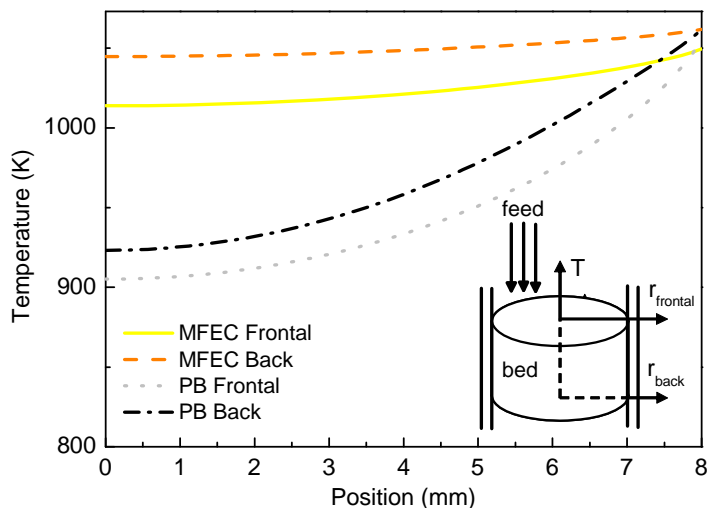
Fig. S5 Temperature profiles at steady-state along the radial direction at frontal and back side of the reaction beds.

As drawn in Fig. S4, the calculated results of reaction rate along the bed were well consistent with the experimental data. So it can be confirmed that this simplified reaction model was applicable for the calculation of temperature distribution inside the reaction bed.
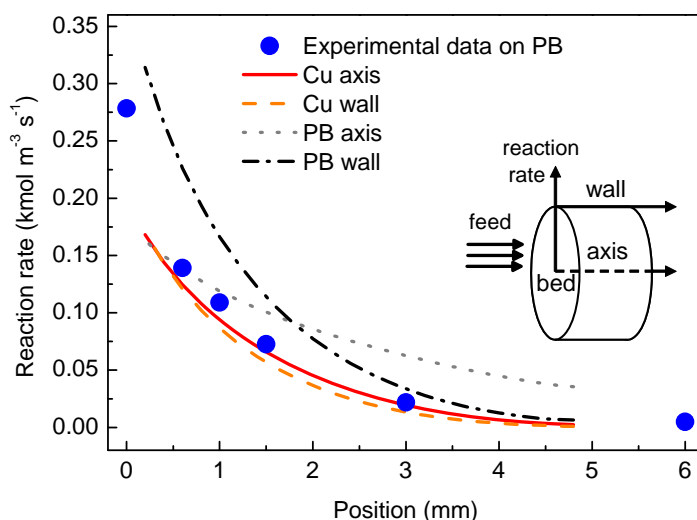
Fig. S6 Reaction rate along the axial direction at wall and central line inside reaction beds.

S4. Images

As shown in Fig. 6S, the individual catalyst particles congregated to large lump due to severe whisker-like carbon formation (inset (b) of Fig 5) after 250 h DRM test.
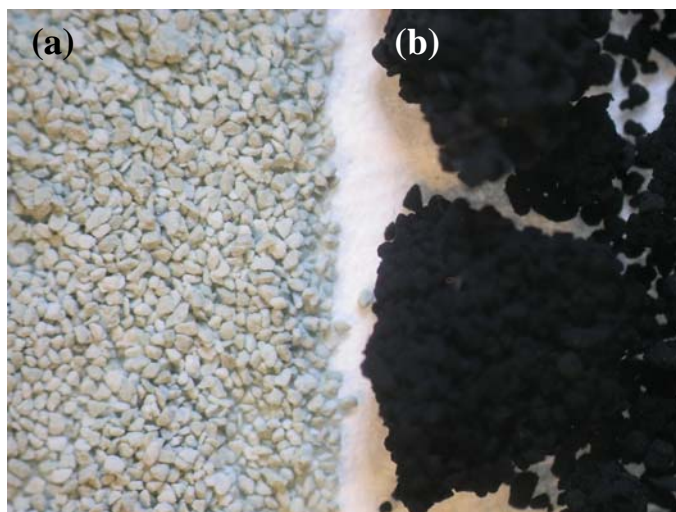
Fig. S7   Optical photograph of the Ni/Al$_2$O$_3$ catalyst sample. (a, left) fresh, and (b, right) used in PB after 250 h DRM at 1073 K using a GHSV of 20,000 mL h^{-1} g$_{cat}$$^{-1}$.

Nomenclature

a	surface to volume ratio of a solid shape (m^2 cm^{-3})
C	constant in equation
	molar concentration (mol m^{-3})
d	diameter (m)
D	diameter of characteristic size of any arbitrary shape (m)
	diffusion coefficient (m^2 s^{-1})
E	internal energy (J kg^{-1})
Ea	apparent activation energy
h^0	enthalpy of formation (J mol^{-1})
h	heat transfer coefficient (W m^{-2} K^{-1})
J	diffusion flux, $\vec{J_i} = -\rho D_{i,m} \nabla Y_i$, (kg m^{-2} s^{-1})
k	thermal conductivity (W m^{-1} K^{-1})
L	length/thickness of reactor bed (m)
n	reaction rate exponent
ΔP	pressure drop (Pa)
R	volumetric rate of reaction (mol m^{-3} s^{-1})
Re	Reynolds number, $Re = \rho u d / \mu$
T	temperature (K)
t	time (s)
u	velocity (m s^{-1})
V	volume (m^3)
X_{FD}	form drag parameter, $X_{FD} = \varepsilon^2/12(1-\varepsilon)$
X	volume fraction in solid
x	volume fraction in bed
Y	mass fraction in gas phase

Greek symbols

γ	turbulence parameter, $\gamma = 2.220\varepsilon_b^2 - 4.575\varepsilon_b + 2.932$
ε	voidage
μ	fluid viscosity (kg m^{-1} s^{-1})
ρ	density (kg m^{-3})
v	stoichiometric coefficient
τ	tortuosity, $\tau_b = \tau_p + \tau_f - 1$,
	$\tau_p = 1+0.49 \ln(1 / 1 - (1 - \varepsilon) X_p)$,
	$\tau_f = 1+1.55 \ln(1 / 1 - (1 - \varepsilon) X_f)$
ϕ	shape factor, $\phi = 6/D_p\, a$

Subscripts

e	effective
f	fluid
i	solid component
j	gas phase species
p	particle
r	radial
s	solid
w	reactor wall
z	axial

References

[S1] Y. Lu, H. Wang, Y. Liu, Q. S. Xue, L. Chen, M. Y. He, *Lab Chip*, 2007, **7**, 133-140.

[S2] M. M. Wang, J. F. Li, L. Chen, Y. Lu, *Int. J. Hydrogen Energy*, 2009, **34**, 1710-1716.

[S3] R. E. Collins, *Flow of fluid through porous materials*, New York: Reinhol, 1961; A. E. Scheidegger, *The physics of flow through porous medium*, University of Toronto Press, 1960.

[S4] S. Ergun, *Chem. Eng. Pro.*, 1952, **48**, 89-94.

[S5] J. F. Li, Ph. D. dissertation, East China Normal University, Shanghai, 2008.

[S6] D. R. Cahela, B. J. Tatarchuk, *Catal. Today*, 2001, **69**, 33-39.

[S7] M. Sheng, H. Y. Yang, D. R. Cahela, B. J. Tatarchuk, *J. Catal.*, 2011, **281**, 254-262.

[S8] E. N. Fuller, P. D. Schettler, J. C. Giddings, *Ind. Eng. Chem.*, 1966, **58**, 19-27.

[S9] M. C. Bradford, M. A. Vannice, *Catal. Rev.-Sci. Eng.*, 1999, **41**, 1-42.